JACS
JOURNAL OF THE AMERICAN CHEMICAL SOCIETY
Article
pubs.acs.org/JACS

Hierarchical Assembly of a $\{Mn^{II}_{15}Mn^{III}_{4}\}$ Brucite Disc: Step-by-Step Formation and Ferrimagnetism

Yong-Kai Deng,[†,∥] Hai-Feng Su,[‡,∥] Jia-Heng Xu,[†] Wen-Guang Wang,[†] Mohamedally Kurmoo,[§] Shui-Chao Lin,[‡] Yuan-Zhi Tan,[‡] Jiong Jia,[†] Di Sun,*[,†,‡] and Lan-Sun Zheng[‡]

[†]Key Lab of Colloid and Interface Chemistry, Ministry of Education, School of Chemistry and Chemical Engineering, Shandong University, Jinan 250100, P. R. China

[‡]State Key Laboratory for Physical Chemistry of Solid Surfaces and Department of Chemistry, College of Chemistry and Chemical Engineering, Xiamen University, Xiamen 361005, People's Republic of China

[§]Institut de Chimie de Strasbourg, Université de Strasbourg, CNRS-UMR 7177, 4 rue Blaise Pascal, 67008 Cedex Strasbourg, France

Supporting Information

ABSTRACT: In search of functional molecular materials and the study of their formation mechanism, we report the elucidation of a hierarchical step-by-step formation from monomer (Mn) to heptamer (Mn_7) to nonadecamer (Mn_{19}) satisfying the relation $1 + \Sigma_n 6n$, where n is the ring number of the Brucite structure using high-resolution electrospray ionization mass spectrometry (HRESI-MS). Three intermediate clusters, Mn_{10}, Mn_{12}, and Mn_{14}, were identified. Furthermore, the Mn_{19} disc remains intact when dissolved in acetonitrile with a well-resolved general formula of $[Mn_{19}(L)_x(OH)_y(N_3)_{36-x-y}]^{2+}$ (x = 18, 17, 16; y = 8, 7, 6; HL = 1-(hydroxymethyl)-3,5-dimethylpyrazole) indicating progressive exchange of N_3^- for OH^-. The high symmetry (R-3) Mn_{19} crystal structure consists of a well-ordered discotic motif where the peripheral organic ligands form a double calix housing the anions and solvent molecules. From the formula and valence bond sums, the charge state is mixed-valent, $[Mn^{II}_{15}Mn^{III}_{4}]$. Its magnetic properties and electrochemistry have been studied. It behaves as a ferrimagnet below 40 K and has a coercive field of 2.7 kOe at 1.8 K, which can be possible by either weak exchange between clusters through the anions and solvents or through dipolar interaction through space as confirmed by the lack of ordering in frozen CH_3CN. The moment of nearly 50 Nμ_B suggests Mn^{II}–Mn^{II} and Mn^{III}–Mn^{III} are ferromagnetically coupled while Mn^{II}–Mn^{III} is antiferromagnetic which is likely if the Mn^{III} are centrally placed in the cluster. This compound displays the rare occurrence of magnetic ordering from nonconnected high-spin molecules.

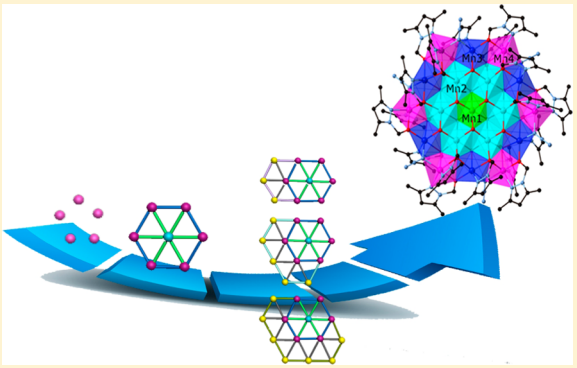

INTRODUCTION

Polynuclear transition metal clusters have captured much attention in the field of molecular magnetism and materials chemistry[1] due to their structural aesthetics and potential applications in areas such as high density data storage,[2] magnetic cooler,[3] and qubits for quantum computation.[4] Since the observation of single-molecule magnetism (SMM) for Mn_{12} in 1990,[5] a whole gamut of polynuclear manganese clusters from Mn_3 to Mn_{84}, as well as other transition and rare-earth metal ions, have been prepared using flexible organic ligands such as carboxylates, β-diketonates and alkoxides.[6] Based on these reported beautiful examples, it is regarded that the small bridging ions are indispensable in aggregating metal ions into clusters, where suitable metal–metal distances for strong magnetic exchange interactions are guaranteed. From a magnetic point of view, OH^-, OR^-, and O^{2-} provide antiferromagnetic M–O–M exchange paths if the angle is >98° and ferromagnetic one for <98°, whereas end-on bridging N_3^- usually resulted in ferromagnetic coupling and hence the spin ground state of a highnuclearity molecule can be increased dramatically.[7] What will happen if OH^-, OR^-, or O^{2-} and N_3^- coexist in a self-assembled system? To find an answer to this question, more examples are highly sought and different bridging ligands need to be explored to address this challenging issue.

On the other hand, the connectivity recognition in a self-assembly process is intensively dependent on the final single crystals obtained by trial and error as well as the X-ray single-crystal diffraction technique, whereas the details of the cluster growth and nucleation process are less known at the molecular level. Electrospray ionization mass spectrometry (ESI-MS) is a powerful tool to precisely determine the elemental composition of the molecular species or assembly intermediates in solutions by matching experimental mass spectra with calculated isotope distributions.[8] The real-time monitoring of the dynamic

Received: November 9, 2015
Published: January 18, 2016

DOI: 10.1021/jacs.5b11736
J. Am. Chem. Soc. 2016, 138, 1328–1334

molecular species in solution by HRESI-MS could provide rich information about bonding and the way reactions progress, which are the deeper aim in chemistry. Cronin's group has exploited the electrospray and cryospray mass spectrometry to track the formation of polyoxometalate (POM), transition metal clusters and exploration of new POMs in solution.[9] Following these works, in 2013, Zeng's group discovered a Co_{16} cluster and tracked its formation and complex elimination and substitution reactions in solution by iterative ESI-MS and crystallography, which provided ample information to understand the complex assembly process.[10] Despite the ever increasing advances in this field,[11] accurate determination of the formula and possible intermediate bridged between initial reactants and final products still represents a major challenge for understanding and exploiting cluster assembly.

Based on the above considerations, we have recently been experimenting with hydroxymethyl-pyrazole ligands in polynuclear cluster chemistry. Such ligands have had limited reports in this area, in comparison to carboxylates and poly alcohols. In this work, we report on this chemistry with Mn(II) in air and obtained an unprecedented mixed-valence hierarchical $(1 + \Sigma_n 6n$, where n is the ring number) homologue of the Brucite heptanuclear[12] cluster (Figure 1) which is the nonadecanuclear

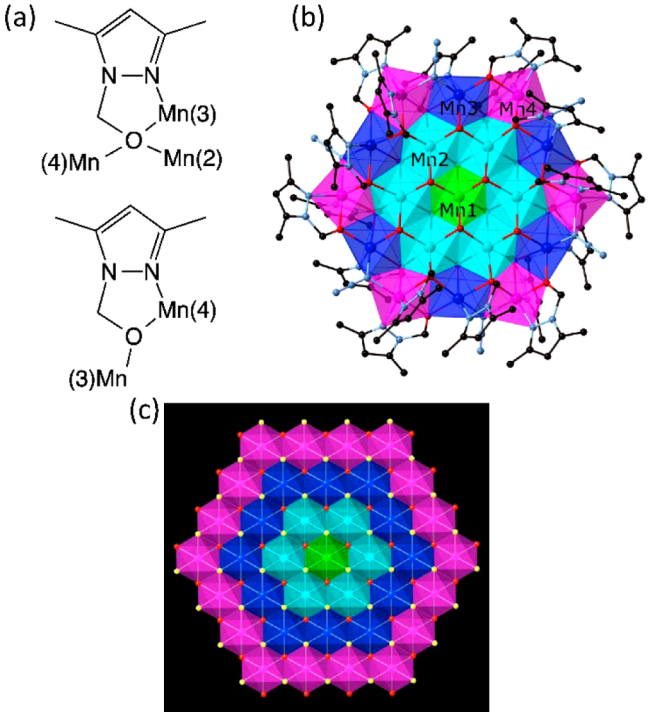

Figure 1. (a) Coordination modes of L^- ligands; (b) structure of a Mn_{19} with three-ring motif; and (c) hierarchy of Brucite discs for $n = 0$ (green), 1 (cyan), 2 (blue), and 3 (purple).

$[Mn^{II}_{15}Mn^{III}_4]$ disc having the formula $[Mn^{II}_{15}Mn^{III}_4(L)_{18}(OH)_{12}(N_3)_6](ClO_4)_6{\cdot}12CH_3CN$ (**1**). More interesting, we examine the solution stability of Mn_{19} disc, indicating the core integrity in acetonitrile and multistep elimination and substitution reaction between coexisted bridging anions. Real-time monitoring of the reaction solution using HRESI-MS at room temperature provided much deeper information about the formation mechanism of this novel Mn_{19} disc, that is, Mn_7 disc is a primary species bridging between single Mn atom and Mn_{19} disc. Surprisingly, Mn_{19} disc in the solid crystalline state does not behave as a SMM as may be expected but displays long-range magnetic ordering to a ferrimagnet at 40 K and a high coercive field of 2.7 kOe at 1.8 K. Both the transition and the magnetic hardness are absent for crystals dissolved in CH_3CN.

RESULTS AND DISCUSSION

Structural Analysis of $[Mn^{II}_{15}Mn^{III}_4(L)_{18}(OH)_{12}(N_3)_6](ClO_4)_6{\cdot}12CH_3CN$ (1). The Mn_{19} cluster was obtained by room temperature reaction of $Mn(ClO_4)_2{\cdot}6H_2O$, NaN_3, and H*L* in CH_3CN with triethylamine as base, and brown crystals of Mn_{19} were grown over a period of 3−4 days. Despite very low yields, it can be readily reproduced. The key feature of the single-crystal structure is the stacking of the discs along the *c*-axis with the ClO_4^- counterions trapped in ellipsoidal cavities between the calix of adjacent clusters and CH_3CN sharing the cavities as well as occupying the interstitial vacancies between the discs (Figure 2a and 2b). **1** crystallized in the trigonal *R*-3

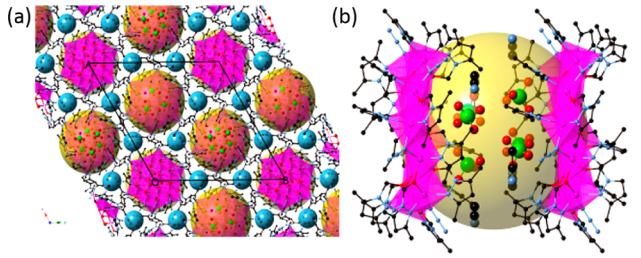

Figure 2. (a) View of the structure along the *c*-axis where the yellow spheres highlight the cavity sandwiched between the adjacent clusters and the gray spheres highlight the channels housing the CH_3CN solvents. (b) Pair of clusters where the calyxes form the cavity (yellow) housing the six ClO_4 and six CH_3CN.

space group with the Mn_{19} disc lying on an inversion center (Figure S1). Its asymmetric unit is one-sixth of the Mn_{19} disc and contains four unique Mn atoms, three L^- ligands, two OH^-, one N_3^-, one ClO_4^- and two CH_3CN solvents. The Mn1 is in an ideal MnO_6 octahedral geometry, as reflected by the six equivalent Mn−O distances of 2.077(5) Å symmetry-imposed by the C_3 axis and the inversion center. The other three Mn atoms are in distorted octahedral geometries and no axial Jahn−Teller effect were observed for all Mn atoms in this disc (Mn−O, 2.062(5)−2.279(5) Å; Mn−O−Mn, 95.67(19)−107.2(2)°; Mn···Mn, 3.2836(11)−3.3723(16) Å; Mn−N−Mn, 99.7(3)°). Although the H atoms of the hydroxide were not located from ΔE-map, several hydrogen bonds were easily identified with ClO_4^-, indicating they are intrinsically hydroxide anions. The 18 L^- ligands sit on the rim above and below the Mn_{19} plane, and are of two types: 6 μ_2-L^- and 12 μ_3-L^-. The Mn_{19} core has S_6 symmetry and can be seen as a three-ring motif: one Mn1 is in the center, which is connected to outer Mn_6 ring (6 Mn2) by six symmetry-related μ_3-OH^- bridges. This Mn_6 ring, in turn, connected to an outermost Mn_{12} ring consisting of alternating Mn3 and Mn4 atoms through alternating μ_3-OH^- and μ_3-O_L (Figure 1). The six end-on μ_2-N_3^- and 12 μ_2-L^- ligands edge-sealed the whole disc at its periphery. Alternatively, this disc also can be described as consisting of 24 edge-sharing $[Mn_3O]$ triangles or 12 edge-sharing $[Mn_4O_2]$ butterfly units. Two discs, acting as calyxes, embrace six ClO_4^- anions, which are hydrogen-bonded with the disc through $O_{hydroxyl}$−H···O hydrogen bonds (O4−H4···O7 = 2.854(12) Å and O5−H5···O6 = 2.854(12) Å).

DOI: 10.1021/jacs.5b11736
J. Am. Chem. Soc. 2016, 138, 1328−1334

In the Mn_{19} disc, charge neutrality requires a total of +42 per 19 Mn atoms. Assuming that the disc comprises Mn atoms in the valence states +2, + 3, and +4, there are three possible valence distributions, $Mn^{II}_{15}Mn^{III}_{4}$, $Mn^{II}_{16}Mn^{III}_{2}Mn^{IV}$, and $Mn^{II}_{17}Mn^{IV}_{2}$. Bond valence sum (BVS) calculations suggest that each Mn atom has a noninteger oxidation state between +2 and +3 (Table S1). Consequently, Mn^{IV} is ruled out. The consideration of overall charge of the nonadecanuclear disc necessitates a mixed-valence $Mn^{II}_{15}Mn^{III}_{4}$ description in accordance with magnetic susceptibility (below). Within the trigonal space group, Mn1 has to be one of the trivalent cation and we assume that the other three are delocalized within the Mn2 ring. The observed solid-state structure suggests rapid intramolecular electron transfer or electron delocalization, which renders Mn^{II} and Mn^{III} indistinguishable on the X-ray time-scale in such highly symmetrical disc. The valence delocalization phenomenon is not at all new in mixed-valence Mn compounds, especially those with high symmetry. For example, in the oxo-centered trinuclear $Mn^{II}Mn^{III}_{2}$ cluster a C_3 axis make the different valence state of Mn atoms became symmetry equivalent.[13] Another $Mn^{II}_{3}Mn^{III}_{4}$ cluster with a symmetry imposed S_6 has valence delocalization feature.[14] Not only limited to metal−organic Mn compounds, this phenomenon also exists in inorganic Mn minerals such as lithiophorite, where Mn^{II} and Mn^{IV} sites are indistinguishable.[15]

Electrospray Ionization Mass Spectrometry. Although so much enthusiasm was poured on the characterization of solid state manganese coordination clusters,[16] their solution behavior and assembly process remain underdeveloped.[17] Mass spectrometry has given very miscellaneous information in coordination chemistry regarding the structural integrity in solution,[18] fragment composition,[19] the degree of protonation,[20] even revelation of the assembly mechanism occurring during the self-assembly process.[21] Crystals of **1** were dissolved in CH_3CN and probed by HRESI-MS at 200 °C. As shown in Figure 3, a series of double charged ion peaks centered in the m/z range of 1840−1960 (max. m/z 1897.080, $[Mn_{19}(L)_{17}(OH)_7(N_3)_{12}]^{2+}$), all of which correspond to a total of nine species with the formulas $[Mn_{19}(L)_x(OH)_y(N_3)_{36-x-y}]^{2+}$ (x = 18, 17, 16; y = 8, 7, 6). Although so many peaks appeared in solution, they belong to the same Mn_{19} species demonstrating clearly that the core of the disc is still intact. The few L^- ligands could be lost from the disc and interesting substitution reaction of the OH^- by N_3^- ions in solution was also observed, which usually occurs during the ESI process as previous reports.[11a,b] There was no evidence of the parent $[Mn_{19}(L)_{18}(OH)_{12}(N_3)_6]^{2+}$ (m/z = 1876.099) cation resulting from **1** by losing all solvent molecules and ClO_4^-, which may be caused by complicated metal−ligand solution exchange between OH^- or L^- and N_3^- ions.

As shown in Figure 3, for doubly charged species, there are nine ion peaks, which can be divided into three subgroups and each subgroup contains three species. Every three ion peaks within a subgroup are formed by replacement of N_3^- by OH^- one by one with the well matched experimental and simulated m/z values. For ion peaks (1), (2), and (3), the former one has a weight of 25 less than the latter one, suggesting a N_3^- (m/z = 42) bridge was replaced by an OH^- (m/z = 17). The other two ionic peaks in each subgroup also show similar substitution reaction and are also unambiguously assigned to precise formulas. Between two adjacent subgroups, the ion peak (3) $[Mn_{19}(L)_{16}(OH)_6(N_3)_{14}]^{2+}$ has a weight of 83 less than that of ion peak (6) $[Mn_{19}(L)_{17}(OH)_6(N_3)_{13}]^{2+}$, representing the replacement of a L^- bridge by N_3^-. Similar behaviors are also observed between ion peak (6) and (9). These results not only clearly proved the existence and stability of the parent Mn_{19} cluster in CH_3CN, but also provided important chemical information about the solution behavior such as ligand exchange in complicated association−dissociation equilibrium in the reaction.

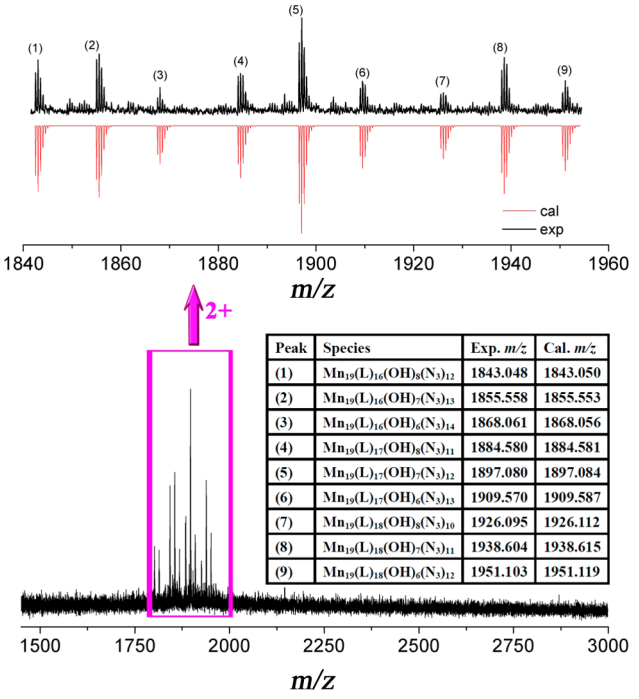

Peak	Species	Exp. m/z	Cal. m/z
(1)	$Mn_{19}(L)_{16}(OH)_8(N_3)_{12}$	1843.048	1843.050
(2)	$Mn_{19}(L)_{16}(OH)_7(N_3)_{13}$	1855.558	1855.553
(3)	$Mn_{19}(L)_{16}(OH)_6(N_3)_{14}$	1868.061	1868.056
(4)	$Mn_{19}(L)_{17}(OH)_8(N_3)_{11}$	1884.580	1884.581
(5)	$Mn_{19}(L)_{17}(OH)_7(N_3)_{12}$	1897.080	1897.084
(6)	$Mn_{19}(L)_{17}(OH)_6(N_3)_{13}$	1909.570	1909.587
(7)	$Mn_{19}(L)_{18}(OH)_8(N_3)_{10}$	1926.095	1926.112
(8)	$Mn_{19}(L)_{18}(OH)_7(N_3)_{11}$	1938.604	1938.615
(9)	$Mn_{19}(L)_{18}(OH)_6(N_3)_{12}$	1951.103	1951.119

Figure 3. HR-ESI mass spectrum of **1** dissolved in acetonitrile. Charge states are indicated as 2+. Experimental (black) and simulated (red) mass spectra of the isotopic envelopes for +2 (top) and +3 (bottom) components. The formula of each species are given in the table.

After checking the solution behaviors of Mn_{19} disc in acetonitrile, we pay attention to the assembly details of such beautiful Mn_{19} disc by tracking the reaction time dependence of the different species present in solution and their abundances from HRESI-MS. The aliquots were taken from the reaction solution at specific time intervals. Each of the aliquots was filtrated and diluted before injecting into the instrument. As shown in Figure 4a, a total of four intermediates and one final product were identified with isotope resolution. The time evolution of HRESI-MS peak intensity is plotted in Figure 4b and the detailed assignment of the main peaks of each species based on experimental and simulated isotope is shown in Supporting Information (Figure S2). Analysis of the HRESI-MS data showed that the very strong double-charged peaks of Mn_7 species were observed in the very short reaction time (approx. the first 1 min), indicating rather quick and high-yield formation of this kinetic product. The most prevailing envelopes in the m/z range of 773−860 are unambiguously assigned to $[Mn_7(L)_7(OH)_2(N_3)_6]^{2+}$, $[Mn_7(L)_8(N_3)_4]^{2+}$, $[Mn_7(L)_8(OH)_2(N_3)_5]^{2+}$, $[Mn_7(L)_9(N_3)_3]^{2+}$, $[Mn_7(L)_9(OH)_2(N_3)_4]^{2+}$, and $[Mn_7(L)_{10}(N_3)_2]^{2+}$ by comparing isotopic distributions. Within the same time window, the low-intensity envelopes of Mn_{10} (11 species identified), Mn_{12} (16 species identified), and Mn_{14} (14 species identified) were also found. This suggests that the further growth of Mn_7 species nearly synchronizes with their formation. It is worth noting that the Mn_{19} species (7 species identified) appears after ~20 min,

DOI: 10.1021/jacs.5b11736
J. Am. Chem. Soc. 2016, 138, 1328−1334

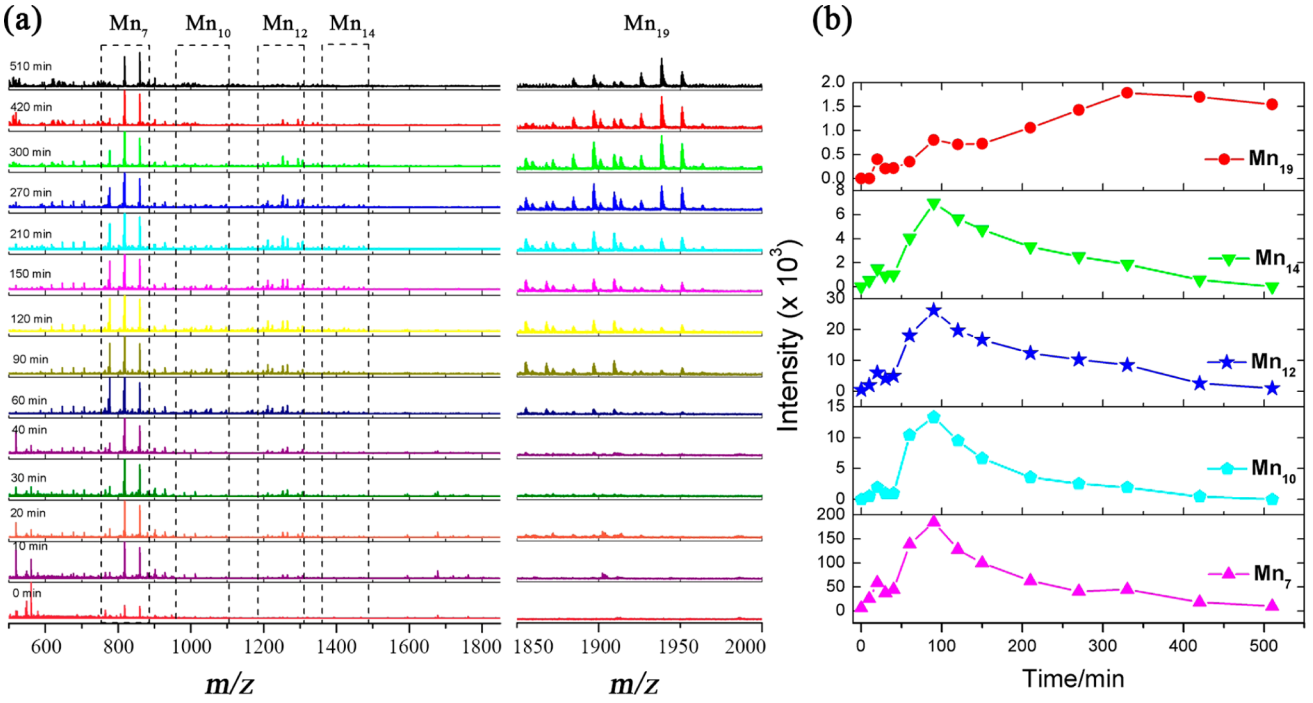

Figure 4. (a) Time-dependent HRESI-MS spectra with five representative Mn_x^{2+} (x = 7, 10, 12, 14 and 19) species. The right panel in (a) is the magnified MS signals of Mn_{19} species (m/z = 1850−2000). (b) HRESI-MS spectral intensity−time profiles of the Mn_x^{2+} species during self-assembly.

although its abundance is very low. During the 20−90 min, the peak intensities of Mn_{10}, Mn_{12}, Mn_{14}, and Mn_{19} species progressively increase and the maximum peak intensities were observed for four smaller intermediates at t = 90 min. As the assembly continued, the peak intensities of Mn_{10}, Mn_{12}, and Mn_{14} species are gradually decreased, whereas intensity of Mn_{19} species increase further to a maximum at t = 330 min, which indicates these smaller intermediates gradually transform to the larger and thermodynamically stable Mn_{19} disc. Based on the real-time HRESI-MS tracking results and the three-ring motif feature of Mn_{19} disc, we tentatively assign its formation to a planar epitaxial growth mechanism from single Mn atom to Mn_7, Mn_{10}, Mn_{12}, and Mn_{14}, then to the final Mn_{19} disc (Scheme 1).

Scheme 1. Schematic View of the Proposed Planar Epitaxial Growth Mechanism of Mn_{19} Core in Solution

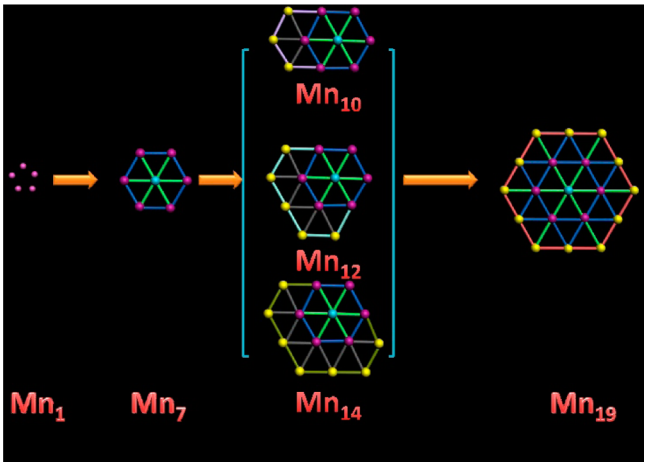

Magnetic Properties. Magnetization data were collected in the temperature range 1.8 and 300 K and field range −70 and +70 kOe (Figure 5). The susceptibility (H = 1 kOe) behaves in a Curie−Weiss fashion with C = 78.74(4) emu K mol^{-1} and θ = −33.1(1) K in the range 100 and 300 K. The Curie constant is close to the 77.6 emu K mol^{-1} expected for 15 Mn^{II} (S = 5/2) and 4 Mn^{III} (S = 2) and assuming g = 2. At 40 K it takes large positive deviation. ZFC-FC magnetizations in 500 Oe show a bifurcation at 40 K and become more divergent below 35 K (Figure 5a). The divergence of the FC magnetization from the ZFC is present for fields of 0.5, 1, 2, and 5 kOe (Figure S3). Plotting $\chi_M T$ versus T shows a minimum of 51.9 emu K mol^{-1} at 48 K (Figure S4), signifying ferrimagnetic behavior.[22] Isothermal magnetizations at 2 K exhibit an almost linear dependence with a slight curvature and attaining 48.3 Nμ_B in 70 kOe (Figure S5), on which is superposed a hysteresis loop. The value of the magnetization of 48.3 Nμ_B in 70 kOe at 1.8 K is smaller than that expected for a ferrimagnet with the moments of 15 Mn^{II} being antiparallel to those of 4 Mn^{III} (15 × 5−4 × 4 = 59 Nμ_B). The hysteresis loop exhibits a coercive field of 2.7 kOe, characterizing it as a moderately hard magnet. The ac-susceptibilities (2 Oe oscillating at different frequencies between 1 and 777 Hz) exhibit peaks for both components at 38 K (Figure S7). The peaks maxima are frequency independent confirming a LRO (long-range ordering) rather than blocking of moments akin a SMM.

The ordering temperature (40 K) is very close to that of the spinel Mn_3O_4 (43 K) and the hysteresis is less (Figure 5b). To demonstrate the intrinsic nature of the LRO, we first confirm the purity of the samples used by PXRD and elemental analyses for CHN and Mn and confirm the absence of biphasic samples using both optical and electron microscopes (Figure S11). We then show that the LRO is absent when dissolved in CH_3CN, reiterating that it cannot be originating from an Mn_3O_4 impurity. Finally we studied a sample of Mn_3O_4 for comparison

DOI: 10.1021/jacs.5b11736
J. Am. Chem. Soc. 2016, 138, 1328−1334

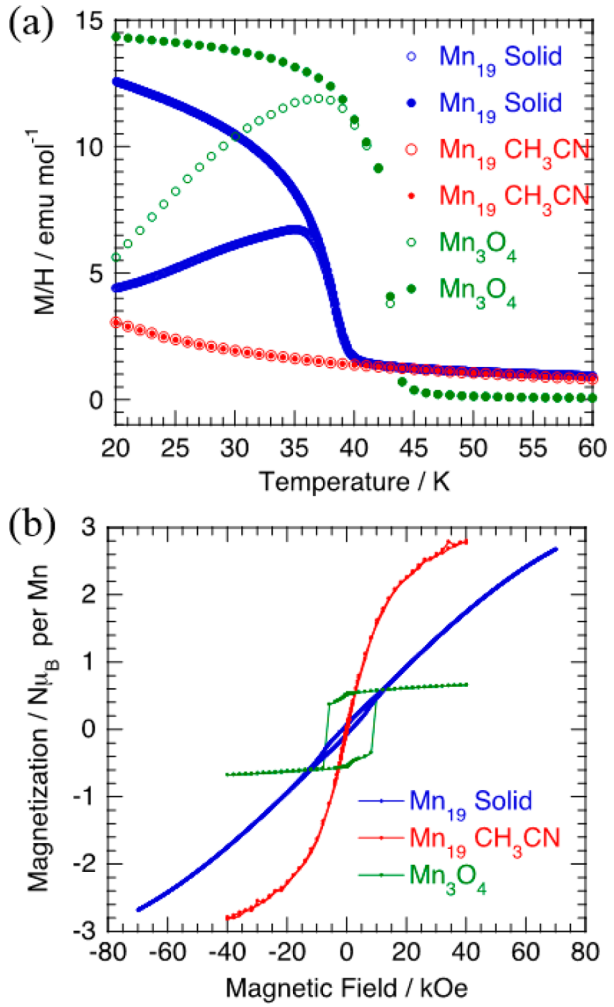

Figure 5. (a) Compared zero-field cooled (hollow circle) and field-cool (solid circle) magnetizations normalized by the field (M/H) in a field of 500 Oe between **1** in solid state, **1** dissolved in CH_3CN, and commercial Mn_3O_4. (b) Isothermal magnetization for a polycrystalline **1** in solid state, **1** dissolved in CH_3CN, and commercial Mn_3O_4 at 1.8 K.

where we estimate that more than 10% of the latter is required to produce a hysteresis of the magnitude observed for **1**.

It is interesting to note that this material is an uncommon magnet where the moment carriers are not connected into infinite lattice. Thus, the ordering can be by one of two mechanisms; first by weak exchange between the discs though the intervening electron densities of the counterions and solvents that are hydrogen-bonded and second, by purely dipolar interaction through space.[22] Due to the high temperature Curie transition, one may bow toward the first the one. In contrast, it is also possible to be the second choice as the moment is fairly high (50 Nμ_B) per disc that are only 8.6 Å between Mn atoms on the edge of adjacent discs and nearest disc to disc distance of 13.5 Å. LRO is destroyed by extending the distance between molecules when the crystals are dissolving in CH_3CN.

In contrast the only known monovalent disc compound,[23] $[Mn^{II}_{19}O_{12}(MOE)_{14}(MOEH)_{10}]\cdot MOEH$ (MOEH = $HOC_2H_5OCH_3$), has almost structurally identical Mn_{19} cores as **1** but lacks the peripheral end-on μ_2-N_3^- bridge. Its magnetism is dominated by antiferromagnetic interaction and neither LRO nor SMM blocking was observed. In the present case, we argue that the $J(Mn^{II}-Mn^{II})$ interaction is ferromagnetic as expected for the end-on μ_2-N_3^- bridge while the $J(Mn^{III}-Mn^{II})$ is antiferromagnetic (Figure S10). The $J(Mn^{III}-Mn^{III})$ exchange will also be ferromagnetic. Consequently, we have a ferrimagnetic cluster which interacts weakly with its neighbors to result in a long-range ordered ferrimagnet. The presence of strong anisotropy originating from the Mn^{III} results in the observed hardness with a coercive field of 2.7 kOe.

Electrochemistry. Cyclic voltammetric studies on **1** were studied in acetonitrile solution containing 0.1 M $^nBu_4NPF_6$ as supporting electrolyte. **1** is only slightly soluble in the electrochemical solvent, and the solution reached saturation at less than the intended 1 mM. The voltammogram of **1** at different scan rates is displayed in Figure 6. For the same

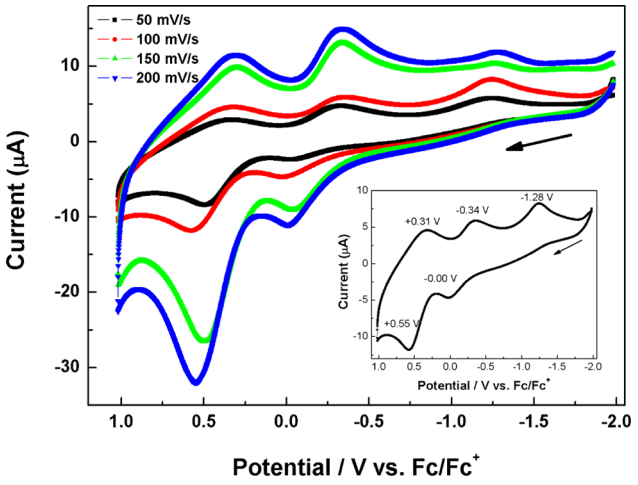

Figure 6. Cyclic voltammogram at different scan rates for **1** in MeCN containing 0.1 M $NBu^n_4PF_6$. Inset: CV at scan rate of 100 mV s^{-1} with labeled potentials.

solution sample, consecutive scans at different rates between −2 and 1 V show the approximately same patterns without other peaks, indicating the absence of any chemical decomposition of **1**. There are three-peak and two-peak patterns for reduction and oxidization sides, respectively. At scan rate of 100 mV s^{-1}, the CV shows two one electron quasi-reversible redox couples at $E_{1/2}$ = 0.43 V (ΔE_p = 0.24 V) and $E_{1/2}$ = −0.17 V (ΔE_p = 0.34 V), and a third irreversible reduction at E_p = −1.28 V (all potentials are referenced to the Fc^+/Fc couple). The profile of the CV traces correspond to multiple Mn^{III}/Mn^{II} couples,[24] which suggests the consecutive electron transfer process occurred in disc core of **1** as summarized in eq 1.

$$Mn^{III}_4Mn^{II}_{15} \overset{0.43V}{\rightleftharpoons} Mn^{III}_3Mn^{II}_{16} \overset{-0.17V}{\rightleftharpoons} Mn^{III}_2Mn^{II}_{17} \overset{-1.28V}{\rightleftharpoons} Mn^{III}_1Mn^{II}_{18} \quad (1)$$

CONCLUSIONS

In this work, we discovered, with the assistance of OH^- and N_3^- bridges, the record size of a mixed-valent Mn disc of Mn_{19}, which exhibits a [1 + 6 + 12] hierarchical arrangement of Mn atoms in a plane. The HRESI-MS results show that **1** maintains the disc integrity in acetonitrile with very complex coordina-

DOI: 10.1021/jacs.5b11736
J. Am. Chem. Soc. 2016, 138, 1328−1334

tion-dissociation equilibrium. The formation of this novel Mn_{19} disc in solution was also monitored by HRESI-MS, which suggests that the Mn_7 disc is a stable and predominant intermediate in solution prior to the step-by-step formation of the Mn_{19} disc, via Mn_{10}, Mn_{12}, and Mn_{14}. The magnetism studies indicated Mn_{19} disc reaches a ferrimagnetic order at a high Curie temperature of 40 K and a coercive field of 2.7 kOe. Current studies not only pave an avenue to such fascinating polynuclear manganese disc but also first discover the assemble intermediates bridged from single Mn atom to the ultimate Mn_{19} disc.

■ ASSOCIATED CONTENT

Supporting Information

The Supporting Information is available free of charge on the ACS Publications website at DOI: 10.1021/jacs.5b11736.

Detailed synthesis procedure, IR, TGA, magnetic plots, BVS calculation, and powder X-ray diffractogram (PDF)
Crystal data (CIF)

■ AUTHOR INFORMATION

Corresponding Author

*dsun@sdu.edu.cn

Author Contributions

‖Y.-K.D. and H.-F.S. contributed equally to this work.

Notes

The authors declare no competing financial interest.

■ ACKNOWLEDGMENTS

This work was supported by the NSFC (Grant Nos. 21201110, 21227001, and 21571115), Young Scholars Program of Shandong University (2015WLJH24), and The Fundamental Research Funds of Shandong University (2015JC045). M.K. is funded by the CNRS, France.

■ REFERENCES

(1) (a) Kurmoo, M. *Chem. Soc. Rev.* **2009**, *38*, 1353−1379. (b) Zhou, Y. L.; Zeng, M. H.; Wei, L. Q.; Li, B. W.; Kurmoo, M. *Chem. Mater.* **2010**, *22*, 4295−4303. (c) Caneschi, A.; Gatteschi, D.; Sessoli, R.; Barra, A. L.; Brunel, L. C.; Guillot, M. *J. Am. Chem. Soc.* **1991**, *113*, 5873−5874. (d) Zheng, Y.; Zhang, Q. C.; Long, L. S.; Huang, R. B.; Muller, A.; Schnack, J.; Zheng, L. S.; Zheng, Z. P. *Chem. Commun.* **2013**, *49*, 36−38. (e) Wei, L. Q.; Zhang, K.; Feng, Y. C.; Wang, Y. H.; Zeng, M. H.; Kurmoo, M. *Inorg. Chem.* **2011**, *50*, 7274−7283. (f) Kong, X. J.; Wu, Y.; Long, L. S.; Zheng, L. S.; Zheng, Z. *J. Am. Chem. Soc.* **2009**, *131*, 6918−6919. (g) Wei, R. J.; Huo, Q.; Tao, J.; Huang, R. B.; Zheng, L. S. *Angew. Chem., Int. Ed.* **2011**, *50*, 8940−8943.

(2) Aromi, G.; Brechin, E. K. *Struct. Bonding (Berlin)* **2006**, *122*, 1−67.

(3) (a) Manoli, M.; Collins, A.; Parsons, S.; Candini, A.; Evangelisti, M.; Brechin, E. K. *J. Am. Chem. Soc.* **2008**, *130*, 11129−11139. (b) Zheng, Y. Z.; Zhou, G. J.; Zheng, Z. P.; Winpenny, R. E. P. *Chem. Soc. Rev.* **2014**, *43*, 1462−1475. (c) Peng, J. B.; Zhang, Q. C.; Kong, X. J.; Ren, Y. P.; Long, L. S.; Huang, R. B.; Zheng, L. S.; Zheng, Z. P. *Angew. Chem., Int. Ed.* **2011**, *50*, 10649−10652.

(4) Tejada, J.; Chudnovsky, E. M.; Del Barco, E.; Hernandez, J. M.; Spiller, T. P. *Nanotechnology* **2001**, *12*, 181−186.

(5) Sessoli, R.; Gatteschi, D.; Caneschi, A.; Novak, M. A. *Nature* **1993**, *365*, 141−143.

(6) (a) Price, J. P.; Batten, S. R.; Moubaraki, B.; Murray, K. S. *Chem. Commun.* **2002**, 762−763. (b) Aromi, G.; Bell, A.; Teat, S. J.; Whittaker, A. G.; Winpenny, R. E. P. *Chem. Commun.* **2002**, 1896−1897. (c) Tasiopoulos, A. J.; Vinslava, A.; Wernsdorfer, W.; Abboud, K. A.; Christou, G. *Angew. Chem., Int. Ed.* **2004**, *43*, 2117−2121. (d) Zaleski, C. M.; Depperman, E. C.; Dendrinou-Samara, C.; Alexiou, M.; Kampf, J. W.; Kessissoglou, D. P.; Kirk, M. L.; Pecoraro, V. L. *J. Am. Chem. Soc.* **2005**, *127*, 12862−12872. (e) Soler, M.; Wernsdorfer, W.; Folting, K.; Pink, M.; Christou, G. *J. Am. Chem. Soc.* **2004**, *126*, 2156−2165. (f) Murugesu, M.; Habrych, M.; Wernsdorfer, W.; Abboud, K. A.; Christou, G. *J. Am. Chem. Soc.* **2004**, *126*, 4766−4767. (g) Maheswaran, S.; Chastanet, G.; Teat, S. J.; Mallah, T.; Sessoli, R.; Wernsdorfer, W.; Winpenny, R. E. P. *Angew. Chem., Int. Ed.* **2005**, *44*, 5044−5048. (h) Moushi, E. E.; Lampropoulos, C.; Wernsdorfer, W.; Nastopoulos, V.; Christou, G.; Tasiopoulos, A. J. *J. Am. Chem. Soc.* **2010**, *132*, 16146−16155.

(7) Papaefstathiou, G. S.; Perlepes, S. P.; Escuer, A.; Vicente, R.; Font-Bardia, M.; Solans, X. *Angew. Chem., Int. Ed.* **2001**, *40*, 884−886.

(8) (a) Miras, H. N.; Wilson, E. F.; Cronin, L. *Chem. Commun.* **2009**, 1297−1311. (b) Rood, J. A.; Boggess, W. C.; Noll, B. C.; Henderson, K. W. *J. Am. Chem. Soc.* **2007**, *129*, 13675−13682. (c) Lim, I. H.; Schrader, W.; Schüth, F. *Chem. Mater.* **2015**, *27*, 3088−3095.

(9) (a) Miras, H. N.; Yan, J.; Long, D. L.; Cronin, L. *Angew. Chem., Int. Ed.* **2008**, *47*, 8420−8423. (b) Miras, H. N.; Cooper, G. J. T.; Long, D. L.; Bogge, H.; Muller, A.; Streb, C.; Cronin, L. *Science* **2010**, *327*, 72−74. (c) Wilson, E. F.; Miras, H. N.; Rosnes, M. H.; Cronin, L. *Angew. Chem., Int. Ed.* **2011**, *50*, 3720−3724. (d) Yan, J.; Long, D. L.; Wilson, E. F.; Cronin, L. *Angew. Chem., Int. Ed.* **2009**, *48*, 4376−4380. (e) Seeber, G.; Cooper, G. J. T.; Newton, G. N.; Rosnes, M. H.; Long, D. L.; Kariuki, B. M.; Kogerler, P.; Cronin, L. *Chem. Sci.* **2010**, *1*, 62−67. (f) Long, D. L.; Streb, C.; Song, Y. F.; Mitchell, S.; Cronin, L. *J. Am. Chem. Soc.* **2008**, *130*, 1830−1832. (g) Newton, G. N.; Cooper, G. J. T.; Kogerler, P.; Long, D. L.; Cronin, L. *J. Am. Chem. Soc.* **2008**, *130*, 790−791.

(10) Zhang, K.; Kurmoo, M.; Wei, L. Q.; Zeng, M. H. *Sci. Rep.* **2013**, *3*, 3516.

(11) (a) Chen, Q.; Zeng, M.-H.; Wei, L.-Q.; Kurmoo, M. *Chem. Mater.* **2010**, *22*, 4328−4334. (b) Zhou, Y. L.; Zeng, M.-H.; Wei, L. Q.; Li, B. W.; Kurmoo, M. *Chem. Mater.* **2010**, *22*, 4295−4303. (c) Wei, L. Q.; Zhang, K.; Feng, Y. C.; Wang, Y. H.; Zeng, M. H.; Kurmoo, M. *Inorg. Chem.* **2011**, *50*, 7274−7283. (d) Zhou, Y. L.; Zeng, M. H.; Liu, X. C.; Liang, H.; Kurmoo, M. *Chem. - Eur. J.* **2011**, *17*, 14084−14093. (e) Xu, F.; Miras, H. N.; Scullion, R. A.; Long, D. L.; Thiel, J.; Cronin, L. *Proc. Natl. Acad. Sci. U. S. A.* **2012**, *109*, 11609−11612. (f) Sun, Q. F.; Murase, T.; Sato, S.; Fujita, M. *Angew. Chem., Int. Ed.* **2011**, *50*, 10318−10321. (g) Fujita, D.; Takahashi, A.; Sato, S.; Fujita, M. *J. Am. Chem. Soc.* **2011**, *133*, 13317−13319. (h) Cui, F. J.; Li, S. G.; Jia, C. D.; Mathieson, J. S.; Cronin, L.; Yang, X. J.; Wu, B. *Inorg. Chem.* **2012**, *51*, 179−187.

(12) (a) Bolcar, M. A.; Aubin, S. M. J.; Folting, K.; Hendrickson, D. N.; Christou, G. *Chem. Commun.* **1997**, *16*, 1485−1486. (b) Chen, S. Y.; Beedle, C. C.; Gan, P. R.; Lee, G. H.; Hill, S.; Yang, E. C. *Inorg. Chem.* **2012**, *51*, 4448−4457. (c) Stamatatos, T. C.; Poole, K. M.; Foguet-Albiol, D.; Abboud, K. A.; O'Brien, T. A.; Christou, G. *Inorg. Chem.* **2008**, *47*, 6593−6595.

(13) Vincent, J. B.; Chang, H. R.; Folting, K.; Huffman, J. C.; Christou, G.; Hendrickson, D. N. *J. Am. Chem. Soc.* **1987**, *109*, 5703−5711.

(14) Abbati, G. L.; Cornia, A.; Fabretti, A. C.; Caneschi, A.; Gatteschi, D. *Inorg. Chem.* **1998**, *37*, 3759−3766.

(15) Wadsley, A. D. *Acta Crystallogr.* **1952**, *5*, 676−680.

(16) (a) Bassil, B. S.; Ibrahim, M.; AlOweini, R.; Asano, M.; Wang, Z. X.; van Tol, J.; Dalal, N. S.; Choi, K. Y.; Biboum, R. N.; Keita, B.; Nadjo, L.; Kortz, U. *Angew. Chem., Int. Ed.* **2011**, *50*, 5961−5964. (b) Xiong, K. C.; Jiang, F. L.; Gai, Y. L.; Yuan, D. Q.; Han, D.; Ma, J.; Zhang, S. Q.; Hong, M. C. *Chem. - Eur. J.* **2012**, *18*, 5536−5540. (c) Zhang, L.; Clerac, R.; Onet, C. I.; Venkatesan, M.; Heijboer, P.; Schmitt, W. *Chem. - Eur. J.* **2012**, *18*, 13984−13988. (d) Zaleski, C. M.; Depperman, E. C.; Kampf, J. W.; Kirk, M. L.; Pecoraro, V. L. *Angew. Chem., Int. Ed.* **2004**, *43*, 3912−3914. (e) Manoli, M.; Inglis, R.; Manos, M. J.; Nastopoulos, V.; Wernsdorfer, W.; Brechin, E. K.; Tasiopoulos, A. J. *Angew. Chem., Int. Ed.* **2011**, *50*, 4441−4444. (f) Langley, S. K.; Stott, R. A.; Chilton, N. F.; Moubaraki, B.; Murray,

DOI: 10.1021/jacs.5b11736
J. Am. Chem. Soc. 2016, 138, 1328−1334

K. S. *Chem. Commun.* **2011**, *47*, 6281−6283. (g) Costa, J. S.; Craig, G. A.; Barrios, L. A.; Roubeau, O.; Ruiz, E.; GomezCoca, S.; Teat, S. J.; Aromi, G. *Chem. - Eur. J.* **2011**, *17*, 4960−4963. (h) Kostakis, G. E.; Ako, A. M.; Powell, A. K. *Chem. Soc. Rev.* **2010**, *39*, 2238−2271. (I) Brechin, E. K.; Clegg, W.; Murrie, M.; Parsons, S.; Teat, S. J.; Winpenny, R. E. P. *J. Am. Chem. Soc.* **1998**, *120*, 7365−7366. (j) Langley, S. K.; Berry, K. J.; Moubaraki, B.; Murray, K. S. *Dalton Trans.* **2009**, 973−982. (k) Ako, A. M.; Hewitt, I. J.; Mereacre, V.; Clerac, R.; Wernsdorfer, W.; Anson, C. E.; Powell, A. K. *Angew. Chem., Int. Ed.* **2006**, *45*, 4926−4929. (l) DendrinouSamara, C.; Alexiou, M.; Zaleski, C. M.; Kampf, J. W.; Kirk, M. L.; Kessissoglou, D. P.; Pecoraro, V. L. *Angew. Chem., Int. Ed.* **2003**, *42*, 3763−3766.

(17) Zhang, L.; Clerac, R.; Heijboer, P.; Schmitt, W. *Angew. Chem., Int. Ed.* **2012**, *51*, 3007−3011.

(18) Song, Y.-F.; Long, D.-L.; Kelly, S. E.; Cronin, L. *Inorg. Chem.* **2008**, *47*, 9137−9139.

(19) (a) Tsunashima, R.; Long, D. L.; Miras, H. N.; Gabb, D.; Pradeep, C. P.; Cronin, L. *Angew. Chem., Int. Ed.* **2010**, *49*, 113−116. (b) Miras, H. N.; Ochoa, M. N. C.; Long, D. L.; Cronin, L. *Chem. Commun.* **2009**, *46*, 8148−8150.

(20) Long, D. L.; Song, Y. F.; Wilson, E. F.; Kogerler, P.; Guo, S. X.; Bond, A. M.; Hargreaves, J. S. J.; Cronin, L. *Angew. Chem., Int. Ed.* **2008**, *47*, 4384−4387.

(21) (a) Wilson, E. F.; Abbas, H.; Duncombe, B. J.; Streb, C.; Long, D. L.; Cronin, L. *J. Am. Chem. Soc.* **2008**, *130*, 13876−13884. (b) Vila-Nadal, L.; Rodriguez-Fortea, A.; Yan, L. K.; Wilson, E. F.; Cronin, L.; Poblet, J. M. *Angew. Chem., Int. Ed.* **2009**, *48*, 5452−5456. (c) Mathey, L.; Paul, M.; Coperet, C.; Tsurugi, H.; Mashima, K. *Chem. - Eur. J.* **2015**, *21*, 13454−13461.

(22) (a) Kurmoo, M. *Chem. Mater.* **1999**, *11*, 3370−3378. (b) Kurmoo, M.; Kumagai, H.; Hughes, S. M.; Kepert, C. J. *Inorg. Chem.* **2003**, *42*, 6709−6722.

(23) Pohl, I. A. M.; Westin, L. G.; Kritikos, M. *Chem. - Eur. J.* **2001**, *7*, 3438−3445.

(24) Alaimo, A. A.; Takahashi, D.; Cunha-Silva, L.; Christou, G.; Stamatatos, T. C. *Inorg. Chem.* **2015**, *54*, 2137−2151. (b) Soler, M.; Chandra, S. K.; Ruiz, D.; Davidson, E. R.; Hendrickson, D. N.; Christou, G. *Chem. Commun.* **2000**, 2417−2418.

DOI: 10.1021/jacs.5b11736
J. Am. Chem. Soc. 2016, 138, 1328−1334